Draft version October 14, 2016
Preprint typeset using LaTeX style emulateapj v. 5/2/11

arXiv:1610.03856v1 [astro-ph.GA] 12 Oct 2016

SPECTROSCOPIC CONFIRMATION OF THE DWARF SPHEROIDAL GALAXY d0944+71 AS A MEMBER OF THE M81 GROUP OF GALAXIES

Elisa Toloba[1,2], David Sand[1], Puragra Guhathakurta[2], Kristin Chiboucas[3], Denija Crnojević[1], and Joshua D. Simon[4]

[1]Texas Tech University, Physics Department, Box 41051, Lubbock, TX 79409-1051, USA
[2]UCO/Lick Observatory, University of California, Santa Cruz, 1156 High Street, Santa Cruz, CA 95064, USA
[3]Gemini Observatory, 670 North Aohoku Pl, Hilo, HI 96720, USA and
[4]Carnegie Observatories, 813 Santa Barbara Street, Pasadena, CA 91101, USA

Draft version October 14, 2016

ABSTRACT

We use Keck/DEIMOS spectroscopy to measure the first velocity and metallicity of a dwarf spheroidal (dSph) galaxy beyond the Local Group using resolved stars. Our target, d0944+71, is a faint dSph found in the halo of the massive spiral galaxy M81 by Chiboucas et al. We coadd the spectra of 27 individual stars and measure a heliocentric radial velocity of -38 ± 10 km s^{-1}. This velocity is consistent with d0944+71 being gravitationally bound to M81. We coadd the spectra of the 23 stars that are consistent with being red giant branch stars and measure an overall metallicity of [Fe/H] $= -1.3 \pm 0.3$ based on the calcium triplet lines. This metallicity is consistent with d0944+71 following the metallicity−luminosity relation for Local Group dSphs. We investigate several potential sources of observational bias but find that our sample of targeted stars is representative of the metallicity distribution function of d0944+71 and any stellar contamination due to seeing effects is negligible. The low ellipticity of the galaxy and its position in the metallicity−luminosity relation suggest that d0944+71 has not been affected by strong tidal stripping.

Subject headings: galaxies: individual (M81, d0944+71) — galaxies: dwarf — galaxies: stellar content – galaxies: kinematics and dynamics – galaxies: evolution

1. INTRODUCTION

Dwarf galaxies play a critical role in our understanding of galaxy formation in the context of the Λ Cold Dark Matter (ΛCDM) paradigm of structure formation. For instance, quantitative verification of the ΛCDM model has struggled in the dwarf-galaxy regime (e.g. the "missing satellites problem", Klypin et al. 1999; Moore et al. 1999; the "too big to fail problem", Boylan-Kolchin et al. 2011, 2012; and apparent planes of satellites, Ibata et al. 2013; Pawlowski et al. 2015), although the most recent numerical simulations make significant progress on several of these issues by including a wide range of baryonic physics (e.g. Brooks & Zolotov 2014; Wetzel et al. 2016). Additionally, the low mass and large numbers of faint dwarf galaxies make them good targets to learn about environmental processes (e.g. tidal and ram pressure stripping), which also makes them vital contributors to the build-up of massive halos (e.g. Johnston et al. 2008). Finally, the star formation histories of Local Volume dwarf galaxies can push the high redshift ultraviolet luminosity function to fainter limits than can direct high redshift constraints (e.g. Weisz et al. 2014).

The challenges to the ΛCDM model on small scales in particular have been largely based on studies in the Local Group, even though a large dispersion in the numbers and properties of dwarf satellites and other halo substructures are expected (e.g. Johnston et al. 2008; Busha et al. 2010). Recent work has thus sought to push the study of faint dwarf galaxies to other Local Volume galaxies (e.g. Chiboucas et al. 2009, 2013; Martínez-Delgado et al. 2015; Merritt et al. 2014; Sand et al. 2015; Carlin et al. 2016, among others), and our own team is conducting the Panoramic Imaging Survey of Centaurus and Sculptor (PISCeS) program in the halos of NGC 5128 and NGC 253 (Sand et al. 2014; Crnojević et al. 2014, 2016; Toloba et al. 2016b).

These studies of faint dwarf galaxy satellites outside the Local Group have largely been photometric in nature, unless there is an accompanying HI neutral gas detection (e.g. Roychowdhury et al. 2012; Sand et al. 2015) or considerable effort is expended to obtain an integrated light spectrum (e.g. van Dokkum et al. 2015, 2016). Spectroscopic information, such as a line of sight velocity and mean metallicity measurement, would add great value to these programs. For instance, dwarf galaxy velocities will be invaluable for investigating the orbital history of satellite systems, the overall halo mass of the primary galaxy and claims of satellite planes. Metallicity measurements would allow for studies of the luminosity – metallicity relation in new environments (Kirby et al. 2011).

We have devised a new method to obtain critical spectroscopic information via resolved stellar populations out to distances of $\sim$ 4 Mpc, utilizing powerful ground-based multi-object spectrographs (as recently described in Toloba et al. 2016a). The method involves co-adding spectra from a single dwarf galaxy or stellar stream to obtain a final spectrum to measure a radial velocity or mean metallicity. Individual slits are placed on carefully chosen stars that are spatially associated with the targeted stellar structure – tip of the red giant branch (TRGB) stars, asymptotic giant branch (AGB) stars and apparent stellar blends – so as to maximize the final signal to noise of the co-added spectrum.

This is the first of a series of papers in which we

toloba@ucolick.org

will analyze the dynamical and metallicity properties of dwarf galaxies and streams that reside in the halos of massive galaxies beyond the Local Group. The spectroscopic subject of this paper is d0944+71, which was discovered by Chiboucas et al. (2009) during a CFHT search for faint dwarf galaxies around M81, and was subsequently confirmed to be at the distance of M81 (D = 3.63 Mpc; Karachentsev et al. 2002) with follow-up *Hubble Space Telescope* observations (Chiboucas et al. 2013). We present several previously known physical properties of d0944+71 in Table 1; it has an absolute magnitude of M_I=−13.2, is gas poor (M_{HI}<3.1×10^5 $M_\odot$; Roychowdhury et al. 2012), and lies at a projected distance of 335 kpc from M81 itself.

2. DATA

2.1. *Observations and Data Reduction*

We designed a slitmask for the DEIMOS spectrograph (Faber et al. 2003) located at the Keck II 10 m telescope in the Mauna Kea Observatory (Hawaii). We used the color-magnitude diagram (CMD) based on *HST*/ACS photometry to select point-like objects that are consistent with being stars in the recently discovered dwarf galaxy d0944+71 in the halo of M81. We selected the closest stars to the tip of the red giant branch ($F814W_{TRGB}$=23.77, extinction corrected; Chiboucas et al. 2013) as spectroscopic targets. Due to the high density of stars, not all the potential targets were observable. Figure 1 shows the position of the 27 observed spectroscopic targets in the CMD and their location in d0944+71.

The observations were carried out using the 1200 lines/mm grating centered at 7800 Å with slit widths of 1.″0 and the OG550 order blocking filter. All the slits were aligned with the mask position angle (P.A. 30°). We integrated for a total of 7.2 hours with an average seeing of 0.9″ on 2016 January 8 − 9. This instrumental configuration provides a wavelength coverage of $\sim 6500 - 9000\mathring{A}$ with a spectral resolution of $R \sim 6000$.

We reduced the data with the SPEC2D pipeline (Cooper et al. 2012; Newman et al. 2013) with modifications described by Kirby et al. (2015a,b). The major improvements consist of improving the wavelength solution by tracing the sky lines along the slit and improving the extraction of the one-dimensional spectra by accounting for the differential atmospheric refraction along the slit. The main steps in the reduction process consisted of flat-field corrections, wavelength calibration, sky subtraction, and cosmic ray cleaning.

2.2. *Observational Biases and Seeing Effects*

We want to use this sample of stars to estimate the radial velocity and metallicity of d0944+71. To know the reliability of our measurements we study how well we are sampling the metallicity distribution function of the dwarf and how much light from other sources contaminates our spectra due to seeing effects.

Our target stars cover the full spatial extent of d0944+71 as shown in Figure 1. Thus, if there is a metallicity gradient within the galaxy, our sample does not favor any particular region.

We test how well our targets represent the bright end of the RGB by calculating the perpendicular distance of each star in the spectroscopic and photometric samples, constrained to the same F814W magnitude range, to the middle isochrone shown in Figure 1. We run a Kolmogorov-Smirnov statistical test and find that we cannot reject the null hypothesis of both samples coming from the same parent sample with a very high confidence ($p - value = 0.58$). If we constrain the parent sample to not only the magnitude but also the color range covered by our targets, the significance level is even higher ($p - value = 0.86$). This means that we sample the metallicity distribution function of d0944+71 for $F814W > 24.39$.

Our RGBs are selected from *HST*/ACS photometry, but our spectroscopy is ground based and therefore affected by seeing. We study how much light from neighboring sources contribute to our spectra by analyzing the sources that are within a radius of our typical seeing (FWHM = 0.9″) centered on our targets. We find that 59% of our RGBs have a light contamination of 0%, 37% of our RGBs have a contamination of < 20%, and 4%, one star, has a luminosity contamination of 45%. This large contribution comes from a background galaxy whose emission lines are clearly seen in our spectrum. This galaxy contributes to the continuum of the spectrum but not to the position of the RGB absorption lines. Thus, this spectrum can be used to measure a radial velocity but not a metallicity. In the remaining cases, the light contamination is null or so low that we do not expect them to affect our spectroscopic measurements.

2.3. *Background and Foreground Contaminants*

Background galaxies with emission lines are visually identified and removed from the sample. We detected one that is co-spatial to an RGB star within our seeing conditions (purple asterisk in Figure 1). Quenched galaxies are not expected within our sample because of their small radii ($R \sim 1$ kpc for compact quenched galaxies at redshift $1 - 2$) with respect to the $\sim$ 0.5 kpc that *HST*/ACS resolves. Smaller galaxies have typical F814W > 26 mag (van der Wel et al. 2014), too faint to have been observed.

We use the Besançon model (Robin et al. 2003) to estimate the number of expected Milky Way stars in the line-of-sight of d0944+71. The model predicts 8 stars with 22 < F814W < 24.5 and 0.6 < F606W − F814W < 1.3 in the *HST*/ACS field-of-view. After applying our specific spectroscopic selection function corresponding to stars near the TRGB, the expected number of MW stars in our sample is < 1. Thus, we do not expect any contaminants within our sample.

We use those regions of the ACS field of view that are furthest from the dwarf to estimate any possible contamination from M81 halo stars, applying our spectroscopic selection function and rescaling the area appropriately, while assuming that any halo contamination at these projected distances from M81 (∼335 kpc) can be approximated by a constant surface density. At most, we estimate a maximum of one star that could be from M81's halo, and we estimate the effects of this potential small contamination in Section 3.1.

3. SPECTROSCOPIC MEASUREMENTS

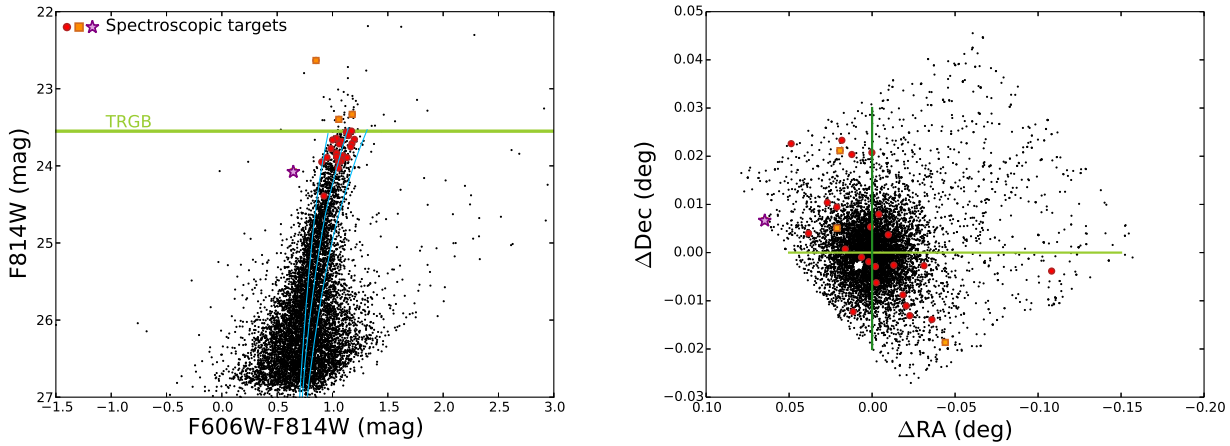

FIG. 1.— Extinction corrected *HST*/ACS CMD and stellar map of d0944+71. Black and colored symbols indicate the location of detected stars in the ACS field of view that are consistent with being in d0944+71. The green line in the left panel indicates the location of the TRGB as calculated by Chiboucas et al. (2013). The green lines in the right panel are lines of PA=0 and 90 degrees. We do not find a velocity change > 22 km s^{-1}with respect to these lines or the lines with PA=45 or 135 degrees. The three blue lines show stellar isochrones from Padova models (Bressan et al. 2012; Marigo et al. 2013; Rosenfield et al. 2016, PARSEC v1.2S+COLIBRI PR16) with an age of 12 Gyr and metallicities of $Z = 0.0001$, $Z = 0.00055$, and $Z = 0.001$ from left to right. The hole close to the center of the galaxy in the right panel coincides with the position of a saturated Milky Way star. The red dots indicate stars that are consistent with being RGB stars. The orange squares indicate stars consistent with being AGB stars. The purple asterisk indicates a star consistent with being a blue loop star that is also blended, due to seeing effects, with a background galaxy.

3.1. *Radial Velocity*

Due to the faintness of the targeted stars, they do not have enough identifiable absorption lines in the individual spectra to obtain a reliable line-of-sight radial velocity (v). To improve the reliability of v we coadd all 27 stars together (see Figure 2). Our spectral coaddition process is the same one as described by Toloba et al. (2016a): (1) correct for possible offsets across the slit using the atmospheric A band seen in the continuum of all objects, this correction is < 10 km s^{-1}; (2) rebin the spectra and their uncertainties to a common wavelength range; (3) renormalize the fluxes and their associated uncertainties; and (4) add, pixel by pixel, the fluxes of the renormalized rebinned spectra by performing a sigma clipping where those pixels that deviate more than 3σ from the median are rejected.

The v of this coadded spectrum is measured using the penalized pixel-fitting (pPXF) method developed by Cappellari & Emsellem (2004). This software finds the composite stellar template that best fits our coadded spectrum. The composite stellar template is a linear combination of the stars in our stellar library (see below) allowing for different weights to minimize template mismatch. Our stellar library consists of 9 high signal-to-noise (S/N $>$ 100) stars of different spectral types (A−K), luminosity classes (I−V), and metallicities ($-3 <$ [Fe/H] < 0) that were observed with the same instrumental configuration.

We computed the uncertainty due to random noise by finding the standard deviation of the velocities of 1000 Monte Carlo realizations of the spectrum. In each realization the spectrum is perturbed pixel by pixel within a Gaussian function whose width is the flux uncertainty. To this random uncertainty we add in quadrature a systematic uncertainty of 1.49 km s^{-1} as estimated by Kirby et al. (2015b). This systematic uncertainty, estimated by comparing repeated measurements of the same stars, includes effects such as uncorrected spectrograph flexure or small errors in the wavelength solution. The measured heliocentric velocity of d0944+71 is -38.3 ± 9.8 km s^{-1}, as shown in Table 1.

In Section 2.3 we determined that we expect to have a maximum of one star from M81's halo contaminating our sample. We estimate the effect that such a star would have on our velocity measurement. The line-of-sight heliocentric velocity of M81 is -36 km s^{-1} and the velocity dispersion in the outer halo is 84 km s^{-1} (Karachentsev et al. 2002). We make two tests: (1) we calculate the line-of-sight velocity after dropping one star at a time from our coadded spectrum and (2) we carry out 100 simulations where we add a random velocity offset within a Gaussian function whose dispersion is 84 km s^{-1} to one star in the coadded spectrum. The dispersion of the 27 velocity measurements for test (1) is 1.7 km s^{-1} and of the 100 simulations of test (2) is 8.7 km s^{-1}. Such small dispersions suggest that a single potential M81 contaminant has no effect on our velocity measurement.

We search for velocity gradients in four different directions (using trial position angles of PA=0, 45, 90, and 135 degrees) given the roundness of this object (see its ellipticity in Table 1). After splitting the velocities into two groups for each trial PA, and searching for differences in velocity between them, no significant gradients were found within the uncertainties. Our data rule out a maximum velocity change of > 22 km s^{-1} and a velocity gradient of > 345 km s^{-1} kpc^{-1}. However, the expected values based on Local Group dSphs of similar luminosity are below our limits (Adén et al. 2009; Ho et al. 2012; Collins et al. 2016), and so this is not a strong constraint.

3.2. *Metallicity*

We estimate the stellar metallicity of d0944+71 following the same procedure as Ho et al. (2015) and Toloba et al. (2016a). This method transforms the equivalent width (EW) of the two strongest absorption

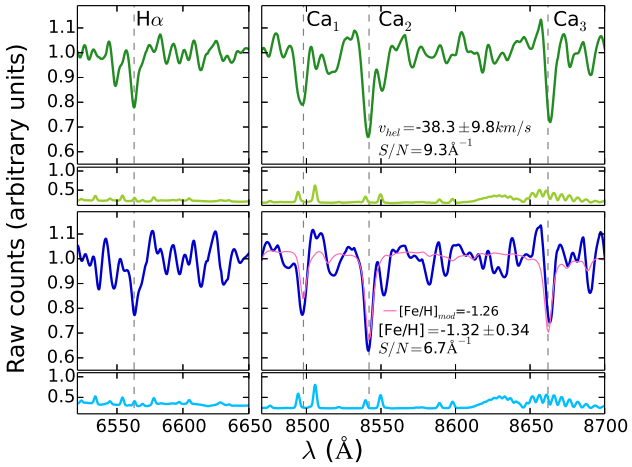

FIG. 2.— Spectra showing the Hα and calcium triplet lines. Upper panels: flux (dark green) and error (light green) spectra that result after coadding all 27 targets used to measure the radial velocity of d0944+71. Lower panels: flux (dark blue) and error (light blue) spectra that result after coadding the 23 targets used to estimate the metallicity (red dots in Figure 1). The pink line is a MIUSCAT model of a single stellar population with age of 14 Gyr and the indicated metallicity for comparison purposes (Vazdekis et al. 2012). The weak Ca_1 line is not used to estimate the metallicity (see Ho et al. 2015).

lines in the calcium triplet into [Fe/H]. These two lines are fitted with a Gaussian function. The measured EW is transformed into the EW value that would have been obtained if we had fitted a Gaussian plus a Lorentzian function. The obtained values are then converted into the total EW of the calcium lines by making an unweighted sum $\Sigma\mathrm{Ca} = \mathrm{EW}_{8542}+\mathrm{EW}_{8662}$, and then transformed into [Fe/H] by using the calibration of Carrera et al. (2013), also used by Ho et al. (2015):

$$[\mathrm{Fe/H}] = -3.51 + 0.12 \times M_I + 0.57 \times \Sigma\mathrm{Ca} - 0.17 \times \Sigma\mathrm{Ca}^{-1.5} + 0.02 \times \Sigma\mathrm{Ca} \times M_I \quad (1)$$

where M_I is the absolute I-band magnitude. The uncertainty in [Fe/H] is the propagation of the uncertainties in ΣCa and M_I accounting for the photometric errors of the I-band magnitudes of the individual stars and the measured distance to d0944+71 by Chiboucas et al. (2013).

Due to the low S/N of the individual spectra, we coadd them together. Yang et al. (2013) demonstrated that when coadding the stars the metallicity measured is the average [Fe/H] of the group of stars. As the calibration above is calculated for RGB stars, we coadd those 23 targets that are consistent with being RGBs (red dots in Figure 1, see the resulting spectrum in Figure 2). M_I, in this case, is the average absolute I-band magnitude of the 23 stars in the coadded spectrum.

We find a metallicity of [Fe/H] = −1.3±0.3, listed in Table 1. It is not possible to measure a metallicity gradient due to the low S/N of the spectra. The photometric metallicity estimated using the full population of detected stars agrees well with the spectroscopic value ($[\mathrm{Fe/H}]_{phot} = -1.3 \pm 0.4$). The estimated photometric metallicity gradient is very mild $d[\mathrm{Fe/H}]/(r/re) \sim 0.06$ dex/re.

Following the same calculations as in Section 3.1 we estimate the effect on our measured metallicity if one M81 halo star were contaminating our sample. The dispersion of the 23 values of [Fe/H] measured after dropping one star at a time from our coadded spectrum is 0.2 dex. However, shifting the velocity of one of the 23 coadded spectra within the dispersion of M81's outer halo introduces an offset in the metallicity towards more metal poor values. We account for these effects in the uncertainties of our quoted metallicity.

TABLE 1
PROPERTIES OF D0944+71

Parameter	Value
RA_0 (hh:mm:ss)(1)	9:44:34.37
DEC_0 (dd:mm:ss)(1)	71:28:55.60
$m - M$ (mag)(1)	$27.87\pm^{0.32}_{0.22}$
D (Mpc)(1)	$3.7\pm^{0.5}_{0.4}$
M_r (mag)(1)	-12.4 ± 0.8
M_I (mag)(1)	-13.2 ± 0.4
M_{HI} ($M_\odot$)(2)	$<3.1\times10^5$
$(V-I)_{TRGB}$(1)	1.13 ± 0.07
r_e (arcsec)(1)	21.4 ± 0.4
r_e (kpc)(1)	0.35 ± 0.02
ϵ(1)	0.11
PA (N to E; deg)(1)	3.6
$\mu_{0,r}$ (mag arcsec^{-2})(1)	23.4
$\langle\mu_{e,r}\rangle$ (mag arcsec^{-2})(1)	23.9
D(M81-d0944+71) (deg)(3)	2.59
D(M81-d0944+71) (Mpc)(3)	0.335
v_{hel} km s^{-1}(4)	-38.3 ± 9.8
ΣCa(4)	5.4 ± 0.6
[Fe/H] (dex)(4)	$-1.3^{+0.3}_{-0.6}$

NOTE. — Rows 1-16 are parameters taken from the literature. Rows 17-19 are derived in this paper.
(1) Parameters from Chiboucas et al. (2013). The central coordinates of the galaxy are in J2000. The magnitudes are measured in the AB system. M_r is measured from ground-based CFHT/MegaCam photometry and M_I from *HST* photometry. The color $V-I$ is calculated in the TRGB. The parameter r_e is the half-light radius, and $\mu_{0,r}$ and $\langle\mu_{h,r}\rangle$ are the central and effective surface brightness.
(2) From Roychowdhury et al. (2012).
(3) Projected distance from M81 to d0944+71.
(4) Heliocentric velocity, total EW of the calcium triplet, and metallicity measured in this work.

4. DISCUSSION AND CONCLUSIONS

We use Keck/DEIMOS spectroscopy to measure the line-of-sight radial velocity and the stellar metallicity of d0944+71, a satellite of the spiral galaxy M81. Due to the faintness of the targeted RGB stars ($22.63 < \mathrm{F814W} < 24.39$) we cannot make spectroscopic measurements in individual stars, but, we can coadd them to obtain average measurements for the dSph.

We coadd a total of 27 stars in d0944+71 and measure a heliocentric radial velocity of −38.3±9.8 km s^{-1}. Including or removing those stars not consistent with being RGB stars in our sample does not change our measured velocities within the uncertainties. This heliocentric velocity is consistent with the velocity of M81 (−36 km s^{-1}; Karachentsev et al. 2002), which is 0.34 Mpc away in projection. This suggests that d0944+71 is likely gravitationally bound to M81.

We coadd 23 RGB stars that span ∼ 0.8 mag below the TRGB to estimate a metallicity of [Fe/H]= −1.3 ± 0.3 based on the calcium triplet lines. The low S/N of

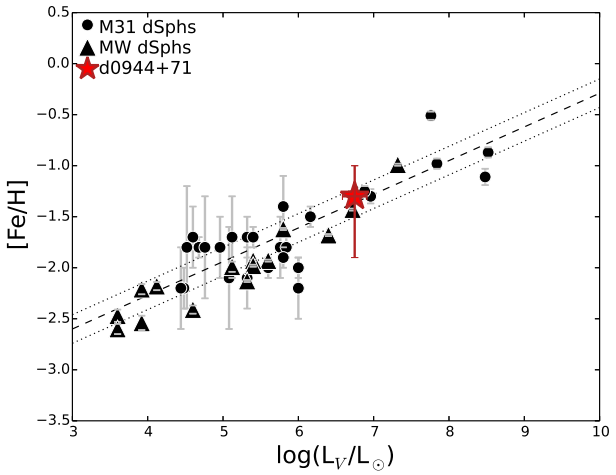

FIG. 3.— Metallicity−luminosity relation for LG dSphs and d0944+71. The measurements for the MW dSphs were done by Kirby et al. (2011) and for M31 dSphs by Collins et al. (2013, 2015); Ho et al. (2015).

our spectra does not allow us to measure a metallicity gradient. This metallicity is consistent with that of Leo I, And VII, and And XVIII, the three Local Group dSphs that have similar luminosity to d0944+71 (Kirby et al. 2011; Collins et al. 2013; Ho et al. 2015).

Figure 3 shows that d0944+71 is consistent with the metallicity−luminosity relation for dSphs in the Local Group. Outliers above the metallicity−luminosity relation are likely galaxies that have been tidally disturbed. In such an event, the galaxy loses stars becoming fainter but keeps the same metallicity if new star formation is not triggered. Outliers below the metallicity−luminosity relation could be explained by internal metallicity gradients. A galaxy with a more metal-poor population in the outskirts would have a more metal-poor measurement than what would have been obtained from a sample of centrally concentrated RGBs. The position of this dSph in the metallicity−luminosity relation in combination with its lack of metallicity gradient measured by the colors of its stars, its roundness, and its lack of tidal disturbances in the spatial distribution of the stars suggest that d0944+71 has not suffered major tidal stripping.

This is the first of a series of papers where we will apply this powerful technique to study the dynamical and metallicity properties of dSph galaxies beyond the Local Group. We will target other galaxies in the M81 group to analyze their orbital properties, the mass of M81, the possible plane where all the satellites lie, and search for dynamical differences between the population of dSphs and dwarf irregulars.

E.T. and P.G. acknowledge the NSF grants AST-1010039 and AST-1412504. D.J.S. is supported by NSF grants AST-1412504 and AST-1517649 and J.D.S. by AST-1412792. The work of DJS was partially performed at the Aspen Center for Physics, which is supported by National Science Foundation grant PHY-1066293. The spectroscopic data presented herein were obtained at the W.M. Keck Observatory, which is operated as a scientific partnership among the California Institute of Technology, the University of California and the National Aeronautics and Space Administration. The Observatory was made possible by the generous financial support of the W.M. Keck Foundation. The authors wish to recognize and acknowledge the very significant cultural role and reverence that the summit of Mauna Kea has always had within the indigenous Hawaiian community. We are most fortunate to have the opportunity to conduct observations from this mountain.

REFERENCES

Adén, D., Wilkinson, M. I., Read, J. I., et al. 2009, ApJ, 706, L150
Boylan-Kolchin, M., Bullock, J. S., & Kaplinghat, M. 2011, MNRAS, 415, L40
Boylan-Kolchin, M., Bullock, J. S., & Kaplinghat, M. 2012, MNRAS, 422, 1203
Bressan, A., Marigo, P., Girardi, L., et al. 2012, MNRAS, 427, 127
Brooks, A. M. & Zolotov, A. 2014, ApJ, 786, 87
Busha, M. T., Alvarez, M. A., Wechsler, R. H., Abel, T., & Strigari, L. E. 2010, ApJ, 710, 408
Cappellari, M. & Emsellem, E. 2004, PASP, 116, 138
Carlin, J. L., Sand, D. J., Price, P., et al. 2016, ApJ, 828, L5
Carrera, R., Pancino, E., Gallart, C., & del Pino, A. 2013, MNRAS, 434, 1681
Chiboucas, K., Jacobs, B. A., Tully, R. B., & Karachentsev, I. D. 2013, AJ, 146, 126
Chiboucas, K., Karachentsev, I. D., & Tully, R. B. 2009, AJ, 137, 3009
Collins, M. L. M., Chapman, S. C., Rich, R. M., et al. 2013, ApJ, 768, 172
Collins, M. L. M., Martin, N. F., Rich, R. M., et al. 2015, ApJ, 799, L13
Collins, M. L. M., Tollerud, E. J., Sand, D. J., et al. 2016, ArXiv e-prints
Cooper, M. C., Newman, J. A., Davis, M., Finkbeiner, D. P., & Gerke, B. F. 2012, spec2d: DEEP2 DEIMOS Spectral Pipeline, astrophysics Source Code Library, ascl:1203.003
Crnojević, D., Sand, D. J., Caldwell, N., et al. 2014, ApJ, 795, L35
Crnojević, D., Sand, D. J., Spekkens, K., et al. 2016, ApJ, 823, 19
Faber, S. M., Phillips, A. C., Kibrick, R. I., et al. 2003, in Society of Photo-Optical Instrumentation Engineers (SPIE) Conference Series, Vol. 4841, Instrument Design and Performance for Optical/Infrared Ground-based Telescopes, ed. M. Iye & A. F. M. Moorwood, 1657–1669
Ho, N., Geha, M., Munoz, R. R., et al. 2012, ApJ, 758, 124
Ho, N., Geha, M., Tollerud, E. J., et al. 2015, ApJ, 798, 77
Ibata, R. A., Lewis, G. F., Conn, A. R., et al. 2013, Nature, 493, 62
Johnston, K. V., Bullock, J. S., Sharma, S., et al. 2008, ApJ, 689, 936
Karachentsev, I. D., Dolphin, A. E., Geisler, D., et al. 2002, A&A, 383, 125
Kirby, E. N., Guo, M., Zhang, A. J., et al. 2015a, ApJ, 801, 125
Kirby, E. N., Lanfranchi, G. A., Simon, J. D., Cohen, J. G., & Guhathakurta, P. 2011, ApJ, 727, 78
Kirby, E. N., Simon, J. D., & Cohen, J. G. 2015b, ApJ, 810, 56
Klypin, A., Kravtsov, A. V., Valenzuela, O., & Prada, F. 1999, ApJ, 522, 82
Marigo, P., Bressan, A., Nanni, A., Girardi, L., & Pumo, M. L. 2013, MNRAS, 434, 488
Martínez-Delgado, D., D'Onghia, E., Chonis, T. S., et al. 2015, AJ, 150, 116
Merritt, A., van Dokkum, P., & Abraham, R. 2014, ApJ, 787, L37
Moore, B., Ghigna, S., Governato, F., et al. 1999, ApJ, 524, L19

Newman, J. A., Cooper, M. C., Davis, M., et al. 2013, ApJS, 208, 5
Pawlowski, M. S., McGaugh, S. S., & Jerjen, H. 2015, MNRAS, 453, 1047
Robin, A. C., Reylé, C., Derrière, S., & Picaud, S. 2003, A&A, 409, 523
Rosenfield, P., Marigo, P., Girardi, L., et al. 2016, ApJ, 822, 73
Roychowdhury, S., Chengalur, J. N., Chiboucas, K., et al. 2012, MNRAS, 426, 665
Sand, D. J., Crnojević, D., Strader, J., et al. 2014, ApJ, 793, L7
Sand, D. J., Spekkens, K., Crnojević, D., et al. 2015, ApJ, 812, L13
Toloba, E., Guhathakurta, P., Romanowsky, A., et al. 2016a, ArXiv e-prints
Toloba, E., Sand, D. J., Spekkens, K., et al. 2016b, ApJ, 816, L5
van der Wel, A., Franx, M., van Dokkum, P. G., et al. 2014, ApJ, 788, 28
van Dokkum, P., Abraham, R., Brodie, J., et al. 2016, ArXiv e-prints
van Dokkum, P. G., Romanowsky, A. J., Abraham, R., et al. 2015, ApJ, 804, L26
Vazdekis, A., Ricciardelli, E., Cenarro, A. J., et al. 2012, MNRAS, 424, 157
Weisz, D. R., Dolphin, A. E., Skillman, E. D., et al. 2014, ApJ, 789, 148
Wetzel, A. R., Hopkins, P. F., Kim, J.-h., et al. 2016, ArXiv e-prints
Yang, L., Kirby, E. N., Guhathakurta, P., Peng, E. W., & Cheng, L. 2013, ApJ, 768, 4